Rare-earth Ferrimagnet based Multilayers [1]

Rare-earth ferrimagnetic thin films have been key materials for magneto-optical recording 3 decades ago. Fig. 1 shows an early magnetic force microscopy study [2] of the contrast reversal of bits on a commercial magneto-optical disk.
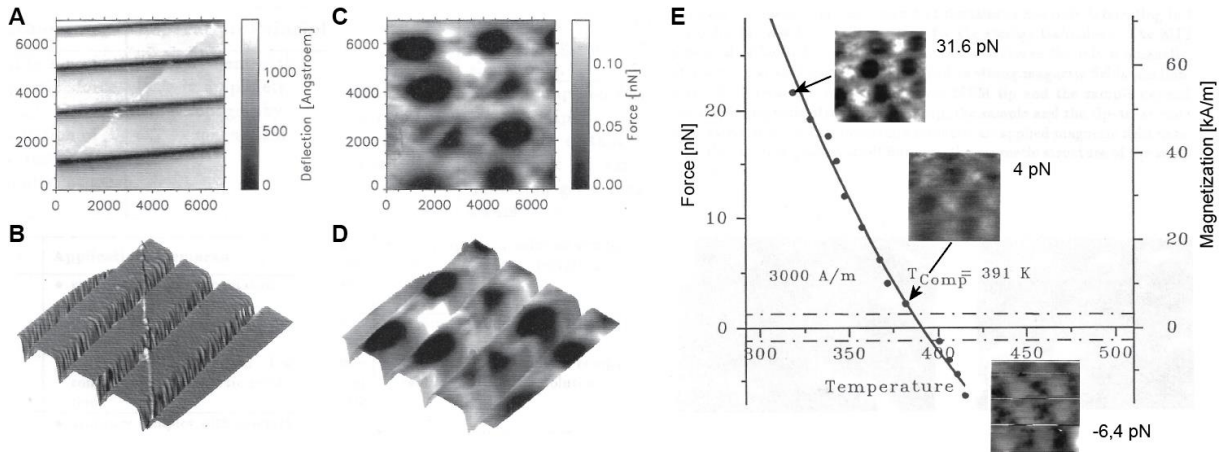

Figure 1: Static MFM measurement [2]. **A** topography of a magneto-optical disk (MOD). **B** 3D rendered image of the topography displayed in **A**. C static mode MFM data. **D** MFM data (**C**) overlaid to the topography (**B**). **E** MFM contrast as a function of sample temperature. Example MFM data is displayed in the three inset figures. For temperatures $T > T_{comp} = 391$ K the sample magnetization is dominated by the CoFe, i.e. $M_{CoFe} > M_{TbFeCo}$. T_{comp} is the compensation temperature.

With rapid development of the storage density of the magnetic hard disks and the growing importance of solid-state memory in personal computing, tablets and smartphones, the magnetism community rapidly lost interest in rare-earth ferrimagnetic thin films.

However, recent discoveries showed that these materials can be used to obtain a giant exchange bias effect [3,4], all optical magnetic writing [5-8], and ultra-fast domain wall devices [9,10] , making this class of thin film materials has relevant topic for the current research. With early work on giant exchange bias [3] we have been among the first groups to focus again on these materials.

First work addressed the giant exchange bias effect that can be obtained with rare-earth transition metal ferrimagnets [3]. To obtain a conventional exchange bias effect, a ferromagnetic film is exchange coupled to an antiferromagnetic thin film (see section on exchange bias). Biasing (a lateral shift of the magnetization loop such that one magnetization is preferred compared to the other) then arises from anchoring the ferromagnet's magnetization in the antiferromagnet, by coupling it to uncompensated spins [11] of the latter, which remain pinned in applied fields [12] and at sufficiently low temperatures. In practice, the density of pinned uncompensated spins is small and thus coupling strength and consequently also the exchange-bias are weak. In our work [3], we reported the observation of large exchange-bias in a perpendicular system using an amorphous Tb-Fe ferrimagnet and a Co/Pt multilayer. Because the Tb moments are expected to align antiparallel to the Fe and Co moments, and, consistently, the Fe moments would align parallel to Co ones, we expect the ferrimagnetic-ferromagnetic coupling to be largely frustration-free and hence strong.
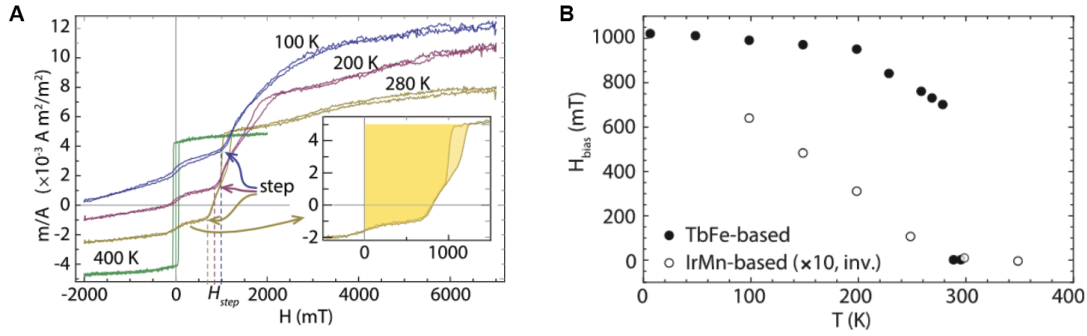
Figure 2: **A** Magnetometry of a $TbFe_{40nm}[Co_{0.4nm}Pt_{0.7nm}]_{x5}$ sample at selected temperatures. Inset: zoom-in on the 280 K loop. The shaded area measures the energy required to magnetize the ferromagnet at that temperature and estimates the strength of its coupling to the ferrimagnet. **B** Exchange-bias as a function of temperature for a conventional MnIr-based system (empty circles) and a TbFe-ferrimagnet based system, (filled circles). For the ease of comparison, the MnIr-system data have been inverted and expanded by a factor of 10.

Fig. 2**A** presents (minor) magnetization loops measured at 100 K, 200 K, and 280 K, whereas Fig. 2B shows the dependence of the exchange bias in a temperature range 7.9–280 for a $TbFe_{40nm}[Co_{0.4nm}Pt_{0.7nm}]_{x5}$ (solid circles) and a conventionally exchange bias sample (empty circles). For the $TbFe_{40nm}[Co_{0.4nm}Pt_{0.7nm}]_{x5}$ sample, an exchange-bias ($\mu_0 H_{ex}$) of 0.7 T is observed at 280 K. A monotonic increase is seen as the temperature is lowered in the range 7.9–280 K. The exchange bias saturates near 1.1 T at 7.9 K. In contrast, H_{ex} in conventional exchange-bias systems obtained with a MnIr antiferromagnet shows no such saturation. H_{ex} in those systems increases continuously with decreasing temperature (empty markers). For ease of comparison, we show inverted values of $\mu_0 H_{ex}$ and use a ten-fold magnified scale.

Note that the magnitude of the exchange-bias in TbFe-based systems is an order of magnitude larger than in conventional systems. This observation is consistent with the view that there is no frustration of the coupling of the TbFe and the Co/Pt layers.

In further work [13] the magnetization process of the soft $[Pt(0.7)/Co(0.4)]_{x5}$ film coupled to the magnetically hard TbFe film was studied by high-resolution magnetic force microscopy at 10.5 K. The magnetization process was found to be surprisingly complex. Instead of the conventional lateral wall motion observed in the soft layer of a weakly exchange-coupled system (see section on exchange bias), a nucleation-dominated three-stage magnetization process showing a significant spatial variation occurs. Fig. 3**A** to **D** show MFM data obtained after cooling the exchange-coupled bilayer system from room temperature to 10.5 K in fields from 0 to 4 T: In stage 1, a granular contrast pattern occurs inside the Co/Pt down domain which increases with the applied field (Fig. 3**A** and **B**). In stage 2, the granular contrast becomes most intensive and a strong evolution of the pattern occurs. Fig. 3**C** shows MFM data taken at a field of 1500 mT, characteristic for stage 2 of the magnetization process. Finally, in stage 3, the contrast of the granular pattern becomes weaker with increasing applied field, but the pattern no longer changes. Fig. 3**D** taken at 4 T shows a typical image of this magnetization 3rd magnetization stage. The characteristic magnetization structures that give rise to these observations can be inferred from matching the simulated MFM $\Delta f(r, z_{ts})$-data based on candidate micromagnetic structures to the measured MFM data. At zero field, the magnetization of Co/Pt multilayer is opposite to that of the ferrimagnetic TbFe layer (Fig. 3**E**). The MFM contrast simulated from this model magnetization pattern is displayed in Fig. 3**I**. Apart from the weak granular structure of the measured image, a good agreement between simulated and measured data is obtained. Note that the granularity arises from grain-to-grain variations of the magnetization or the misalignment of the grains' easy axis with the z-direction which are both not considered in the candidate magnetization structure.
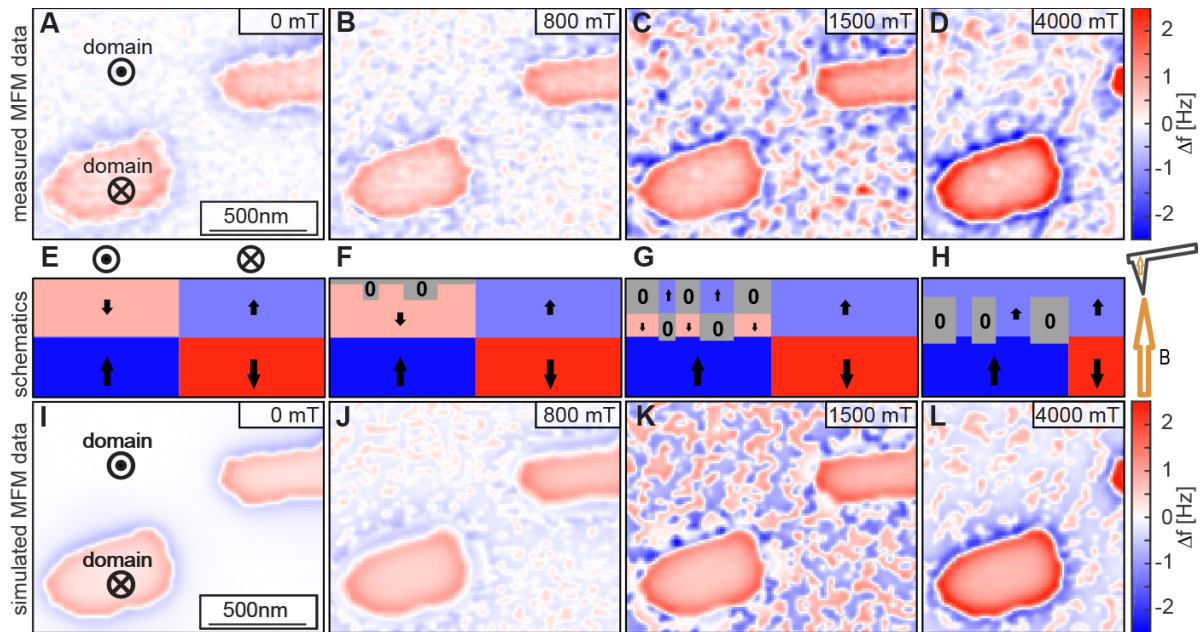
Figure 3: Comparison of modeled (panels in the second row) and measured (panels in the third row) MFM data. **A** - **D** measured MFM images. **E** – **H** Schematics of candidate magnetization structures used for modeling the MFM contrast of the different magnetization stages. **I** - **L** Simulated MFM images obtained from the candidate magnetization structures.

In stage 1, the gradual increase of the contrast is compatible with a rotation of the initially down magnetic moments of Co/Pt toward the field (up) direction. Because the magnetic moments of the Co/Pt multilayer at the interface are pinned to the magnetic moments of the high-anisotropy TbFe film, the Co/Pt multilayer magnetic moments at the top surface are expected to rotate more than those near the interface. For the modeling of the MFM contrast, the vertical structure of the spin chains at any given location on the image plane is modeled by a corresponding spatial distribution of "subdomain blocks" with zero magnetization, located at the top of the Co/Pt multilayer and reaching into different depths toward the interface (gray blocks in Fig. 3**F**). The lateral distribution of these blocks can be inferred from the granular contrast observed in the MFM $\Delta f(r,z_{ts})$-data displayed in Fig. 3**B**). With optimized sublayer depths, again an excellent agreement between the modeled and measured MFM $\Delta f(r,zts)$-data could be obtained.

In stage 2, a strong increase of the contrast is accompanied with a substantial change of the appearance of the granular pattern. These observations are compatible with isolated Co/Pt grains switching their magnetization from a canted down to a canted up state (as was used in our modeling). This is reminiscent of a Stoner-Wohlfarth magnetization process with a field applied away from the easy axis where an instability of the magnetization state occurs. The candidate magnetization structure for stage 2 is depicted in Fig. 3**G**). With the latter, an excellent agreement of the modeled Fig. 3**K**) with the measured MFM $\Delta f(r,z_{ts})$-contrast (Fig. 3**C**) could again be obtained.

In the third magnetization stage (2000 mT< B ≤ 7000 mT see for example Fig. 3**D**), the pattern of the granular contrast inside the up domain no longer changes, and a reduction of its contrast in increasing fields is observed. This behavior is compatible with compression of an interfacial domain wall that forms at the bottom and top of the ferromagnetic and ferrimagnetic layers, respectively. As the Co/Pt multilayer approaches saturation, its magnetic moment distribution becomes more homogeneous and its stray field thus decays (note that the stray field of a layer with a homogeneous magnetization vanishes). Fig. 3**H**) shows the model magnetization distribution to obtain the simulated MFM image displayed in Fig. 3**L**) with the measured data shown in Fig. 3**D**).

To better understand the nucleation-governed magnetization process, micromagnetic modeling was performed by our collaborators, Dr. Christoph Vogler and <u>Prof. Dr. Dieter Süss</u> of the

Vienna University. In this study, two different approaches were used. In the first approach a one-dimensional spin-chain model was implemented to explain the magnetization behavior of isolated grains. The 3-stage magnetization process inferred from the MFM observation and modeling of the MFM contrast could be confirmed. In the second modeling approach, a full 3D-micromagnetic calculation was performed. The result showed that the magnetization behavior can be well understood with the simpler one-dimensional spin chain model and therefore justified the trivial candidate magnetization structures used for the simulation of the observed MFM images.

Recent work submitted by Dr. Christoph Vogler [14], the occurrence of completely reversible, hysteresis-free minor loops of $[Co(0.2)/Ni(0.4)/Pt(0.6)]_N$ multilayers exchange-coupled to a 20 nm thick ferrimagnetic $Tb_{28}Co_{14}Fe_{58}$ layer was demonstrated. In addition, a detailed theoretical investigation by means of micromagnetic simulations done which resulted in an analytical derivation for the condition of the occurrence of full reversibility in magnetization reversal.

In further a work [15], which was recently submitted, we address "Pervasive artifacts revealed from magnetometry measurements of rare earth-transition metal thin films". We found that a class of artifacts manifesting as soft magnetic components in magnetometry measurements of rare earth-transition metal (TbFe) thin films prepared by magnetron sputtering. These artifacts are not inherent to TbFe, but are a direct result of the manner in which the substrates are mounted prior to sample fabrication, with material deposited at the substrate sides giving rise to a significant magnetic moment. We found the same artifacts to also be present in rare earth-free [Co/Pt] multilayers. Trying to suppress the appearance of this type of artifacts has an in influence on the coercivity and, in some cases, on the shape of the reversal curves. Care needs to be taken during fabrication to ensure reliable and reproducible samples so that sensitive magnetic parameters, such as coercivity and compensation points, can be extracted accurately and that data is not misinterpreted for even more complex systems. This type of artifact is not limited to the samples prepared by sputtering, but can extend to other conventional thin-film deposition methods.

References:

[1] This project was financially supported by SNF projects 200021_147084 and 200021E-160637

[2] MFM data by H.J. Hug performed 1992 at the Department of Physics of the Basel University, Switzerland.

[3] Romer, S., Marioni, M. A., Thorwarth, K., Joshi, N. R., Corticelli, C. E., Hug, H. J., et al. (2012). *Temperature dependence of large exchange-bias in TbFe-Co/Pt.* Applied Physics Letters 101, 222404. http://doi.org/{10.1063/1.4767142}

[4] Schubert, C., Hebler, B., Schletter, H., Liebig, A., Daniel, M., Abrudan, R., et al. (2013). *Interfacial exchange coupling in Fe-Tb/[Co/Pt] heterostructures.* Physical Review B, 87(5), 054415–9. http://doi.org/10.1103/PhysRevB.87.054415

[5] Kim, J.-W., Lee, K.-D., Jeong, J.-W., & Shin, S.-C. (2009). *Ultrafast spin demagnetization by nonthermal electrons of TbFe alloy film.* Applied Physics Letters, 94(19), 192506. http://doi.org/10.1063/1.3130743

[6] Ostler, T. A., Barker, J., Evans, R. F. L., Chantrell, R. W., Atxitia, U., Chubykalo-Fesenko, O., et al. (2019). *Ultrafast heating as a sufficient stimulus for magnetization reversal in a ferrimagnet.* Nature Communications, 3(1), 1–6. http://doi.org/10.1038/ncomms1666

[7] Hassdenteufel, A., Hebler, B., Schubert, C., Liebig, A., Teich, M., Helm, M., et al. (2013). *Thermally Assisted All-Optical Helicity Dependent Magnetic Switching in Amorphous $Fe_{100-x}Tb_x$ Alloy Films.* Advanced Materials, 25(22), 3122–3128. http://doi.org/10.1002/adma.201300176

[8]   Graves, C. E., Reid, A. H., Wang, T., Wu, B., De Jong, S., Vahaplar, K., et al. (2013). *Nanoscale spin reversal by non-local angular momentum transfer following ultrafast laser excitation in ferrimagnetic GdFeCo.* Nature Materials, 12(4), 293–298. http://doi.org/10.1038/nmat3597

[9]   Kim, K.-J., Kim, S. K., Hirata, Y., Oh, S.-H., Tono, T., Kim, D.-H., et al. (2017). *Fast domain wall motion in the vicinity of the angular momentum compensation temperature of ferrimagnets.* Nature Materials, 16(12), 1187–1192. http://doi.org/10.1038/nmat4990

[10] Li, W. H., Jin, Z., Wen, D. L., Zhang, X. M., Qin, M. H., & Liu, J. M. (2020). *Ultrafast domain wall motion in ferrimagnets induced by magnetic anisotropy gradient.* Physical Review B, 101(2), 214. http://doi.org/10.1103/PhysRevB.101.024414

[11] Takano, K., Kodama, R. H., Berkowitz, A. E., Cao, W., & Thomas, G. (1997). Interfacial Uncompensated Antiferromagnetic Spins: Role in Unidirectional Anisotropy in Polycrystalline Ni81Fe19/CoO Bilayers. Physical Review Letters, 79(6), 1130–1133. http://doi.org/10.1103/PhysRevLett.79.1130

[12] Kappenberger, P., Martin, S., Pellmont, Y., Hug, H. J., Kortright, J. B., Hellwig, O., & Fullerton, E. E. (2003). Direct imaging and determination of the uncompensated spin density in exchange-biased CoO/(CoPt) multilayers. Physical Review Letters, 91(26), 267202. http://doi.org/10.1103/PhysRevLett.91.267202

[13] Zhao, X., Mandru, A. O., Vogler, C., Marioni, M. A., Suess, D., & Hug, H. J. (2019). *Magnetization Reversal of Strongly Exchange-Coupled Double Nanolayers for Spintronic Devices.* ACS Applied Nano Materials, 2(12), 7478–7487. http://doi.org/10.1021/acsanm.9b01243

[14] Vogler, C., Heigl, M., Zhao, X., Mandru, A. O., Hebler, B., Marioni, M. A., Hug, H. J., Albrecht, M., & Suess, D., (2020). *Hysteresis-free switching of multilayer grains with finite magnetic anisotropy.* Submitted.

[15] Mandru, A. O., Yildirim O., Marioni, M. A., Rohrmann, H., Heigl, M., Ciubotariu, O.-T., Penedo, M., Zhao, X., Albrecht, M., & Hug, H. J., (2020). *Pervasive artifacts revealed from magnetometry measurements of rare earth-transition metal thin films*. Submitted.